International Journal of Thermophysics, Vol. 25, No. 4, July 2004 (© 2004)

Quasi-Steady State Method: Uncertainty Assessment[1]

U. Hammerschmidt[2]

The newly developed quasi-steady state (QSS) method to measure the thermal conductivity combines characteristic advantages of transient and steady-state techniques but avoids their major drawbacks. Based upon a transient hot strip setup, the QSS technique can be realized by adding only two temperature sensors at different radial distances from the strip. After a short settling time, the QSS output signal which is the measure for the thermal conductivity is constant in time as it is for steady-state instruments. Moreover, in contrast to transient techniques, the QSS signal is not altered by homogeneous boundary conditions. Thus, there is no need to locate a time window as has to be done with the transient hot wire or transient hot strip techniques. This paper describes the assessment of the QSS standard uncertainty of thermal conductivity according to the corresponding ISO Guide. As has already been done in previous papers on the uncertainty of the transient hot wire and transient hot strip techniques, first, the most significant sources of error are analyzed and numerically evaluated. Then the results are combined to yield an estimated overall uncertainty of 3.8%. Simultaneously, the present assessment is used as an aid in planning an experiment and in designing a QSS sensor to achieve minimal uncertainty. Such a sensor is used to verify the above mentioned standard uncertainty from a run on the candidate reference material polymethyl methacrylate.

KEY WORDS: boundary condition; ISO GUM; polymethyl methacrylate; quasi-steady state technique; sensor design; standard uncertainty; thermal conductivity; transient hot strip; transient hot wire.

1. INTRODUCTION

The thermal conductivity, λ, is experimentally determined from the response of the temperature of the medium under test to an imposed

[1]Paper presented at the Fifteenth Symposium on Thermophysical Properties, June 22–27, 2003, Boulder, Colorado, U.S.A.

[2]Physikalisch-Technische Bundesanstalt, Bundesallee 100, D-38116 Braunschweig, Germany. E-mail: ulf.hammerschmidt@ptb.de

0195-928X/04/0700-1163/0

known rate of heat flow. The observed temperature may be either constant or variable with time. According to this nature, measuring methods can be grouped into two classes: steady-state and transient techniques.

Now, there is a third class in between, the quasi-steady state (QSS) technique [1]. This method allows a *transient* operating instrument to generate a *steady-state* temperature response. This output signal is a direct measure of the thermal conductivity. Based upon a conventional transient hot wire (THW) or transient hot strip (THS) arrangement, the QSS technique can be realized by simply adding one thermometer. The difference in the temperatures of this thermometer and the wire or strip becomes constant after a short settling time, independent of the dynamic temperature field within the specimen [1]. Moreover, as has been shown in Ref. 1, homogeneous boundary conditions do not affect the QSS. Thus, there is no need for guard heaters as with steady-state apparatuses or for locating a proper time window to evaluate the output signal of transient instruments [1, 2]. Hence, according to the QSS, an indicating thermal conductivity meter can be built.

Whenever a new technique is available in addition to well-established other methods for the same task, frequently there is the question as to which one will produce the best results, i.e., results of the least uncertainty. The problem can readily be solved by uncertainty analyses of the competing methods, such as in the present case, the transient hot wire and hot strip techniques and, e.g., the steady-state guarded hot plate methods. The uncertainties of the three methods mentioned have meanwhile been assessed by the same author [2–4] following the ISO GUM [5]. For the hot plate instrument of Physikalisch–Technische Bundesanstalt (PTB) a standard uncertainty of 1.9% has been estimated while for the other two transient techniques, 5% (THS) and 5.8% (THW) have been found.

In this paper, the uncertainty of the QSS technique will be assessed according to the ISO GUM and compared to already published data of three comparable instruments. First, the theoretical background will briefly be reviewed to identify the underlying simple physical principles. The main body of the paper then proceeds as has been done with the three uncertainty assessments mentioned; a general uncertainty analysis is performed analyzing three types of major errors caused by the model, the evaluation procedure, and the measuring instruments. The sensitivity of the result to errors of the measurement inputs is quantified. From the identified uncertainty magnification factors, design criteria for the QSS λ-sensor used and the experiment are derived.

Although the new technique can also be applied to liquids and gases, the investigations here are restricted to solids. Experiments on polymethyl methacrylate, a candidate reference material, confirm the results.

2. THEORY

The ideal physical model of the QSS technique is that of an embedded infinite line or strip heat source that liberates its constant rate of heat flow, Φ, entirely to the surrounding cylindrical medium of finite radius R. At this point, it should be emphasized, that the latter condition, a *finite* medium, is distinct from the ideal models of the transient hot wire and transient hot strip techniques that require an unbounded surrounding medium. Apart from that, the fundamental THW model is taken as a basis of the QSS method. It will be shown that this model can be applied to the THS technique with only minor modifications.

The theory of the transient hot wire technique is presented in detail elsewhere [e.g., Refs. 3 and 6–8]. In this technique, a line source of constant strength per unit length, Φ/L, liberates its heat to an unbounded specimen of constant thermal conductivity λ and thermal diffusivity a. The resulting temperature rise, $\Delta T(r, t) = T(r, t) - T_0$, of the specimen at time t and position r is governed by

$$\Delta T(r, t) = \frac{\Phi}{4\pi L\lambda}\left[-\mathrm{Ei}\left(-\frac{r^2}{4at}\right)\right], \tag{1}$$

where $T_0 = T(r, t=0)$ is the initial temperature. In practice, the rate of heat flow, $\Phi = U I_0$, is generated by a Joule heated wire of voltage drop U due to an imposed electrical current I_0. The exponential integral, $-\mathrm{Ei}(-z) \equiv \mathrm{E}_1(z)$, can be expanded into a McLaurin series. Retaining the first four terms results in

$$\Delta T(r, t) \approx \frac{\Phi}{4\pi L\lambda}\left[-\gamma - \ln\left(\frac{r^2}{4at}\right) + \frac{r^2}{4at} - \frac{1}{4}\left(\frac{r^2}{4at}\right)^2\right]. \tag{2}$$

For

$$\frac{at}{r^2} \gg 1, \tag{3}$$

all terms of the series vanish except the first two for which γ is Euler's constant. Both of these terms contribute to the standard working equation of the transient hot wire technique

$$\Delta T(r, t) = \frac{\Phi}{4\pi L\lambda}\ln\left(\frac{4at}{Cr^2}\right), \tag{4}$$

where $C = \exp\gamma = 1.781\ldots$

The QSS working equation is easily found by calculating the temperature difference, $T(r_1, t) - T(r_2, t)$, between two stations T1 and T2 at $r = r_1$ and $r = r_2 = \varepsilon r_1 (\varepsilon > 1)$, respectively,

$$\Delta' T = \frac{\Phi}{4\pi L \lambda} \ln \frac{r_2^2}{r_1^2} = \frac{\Phi}{4\pi L \lambda} \ln \varepsilon^2. \tag{5}$$

(Substituting $r_2 = R$ (outer radius of the cylindrical specimen), yields, as a special case, the working equation of the steady-state mode.) As discussed in detail in Ref. 2, Eq. (5) is practically not valid before the time,

$$t_{\min}^{\mathrm{W2}} \geqslant 9 \frac{r_2^2}{a}, \tag{6}$$

because of the truncation of the above series. The superscript "W2" stands for "wire/thermometer T2". The upper time limit of Eq. (5) is discussed below.

Equation (5) can be solved for λ by simply rearranging it

$$\lambda = \frac{\Phi}{4\pi L \Delta' T(t)} \ln \varepsilon^2, \quad \Phi = U I_0. \tag{7}$$

In this equation, it is assumed that

$$\varepsilon = \frac{r_2}{r_1} > 1, \tag{8}$$

Since $\Delta' T = \Delta' T(t)$, in Eq. (7) the quantity to be measured, $\lambda = \lambda(t)$, appears as a pseudo-function of time t.

Due to the finite speed of propagation of heat in solids and fluids, the difference in the individual distances of the two thermometers from the source causes a shift in their quasilinear response times, $\Delta \ln t$. This period in time can be expressed as follows [cf. Ref. 9]:

$$\Delta \ln t = \ln t_{T_2} - \ln t_{T_1} = \ln \left(\frac{r_2}{r_1} \right)^2 = 2 \ln \varepsilon \tag{9}$$

or

$$\frac{\ln r_2 - \ln r_1}{\ln t_{T_2} - \ln t_{T_2}} = \frac{1}{2}. \tag{10}$$

The mutual shift, $\Delta \ln t$, does not depend on the thermal diffusivity of the medium. From Eq. (10) it follows that

$$\frac{r_2}{r_1} = \sqrt{\frac{t_{T_2}}{t_{T_1}}}. \tag{11}$$

Equation (9) is substituted into Eq. (7) to solve for the experimental result

$$\lambda = \frac{\Phi}{4\pi L \Delta' T} \Delta \ln t. \tag{12}$$

This result is the time-equivalent of the above basic QSS working equation, Eq. (7). The thermal conductivity measured is assigned to the working temperature, T_W, which is the mean of the temperatures of the two stations T1 and T2

$$T_W = \frac{T(r_1, t) + T(r_2, t)}{2}. \tag{13}$$

Typical temperature excursions, $T(r_1, t)$ and $T(r_2, t)$, of thermometers T1 and T2 have been calculated for a given parameter set to Eq. (1). Both curves, W1 and W2, can be seen in Fig. 1 together with their QSS signal, WD, according to Eq. (5). The QSS mode with its time invariant output signal starts as soon as the input signal of the second thermometer at $r = r_2$ begins to rise sufficiently linear in $\ln t$ (cf. Eq. (6)). However, in contrast to both its constituents, the QSS signal practically is not altered

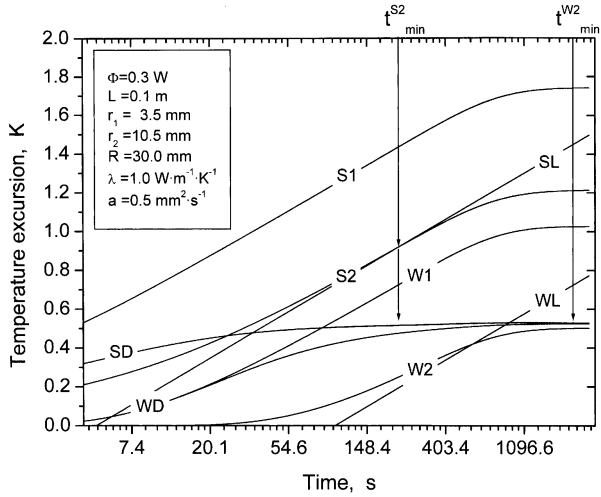

Fig. 1. Calculated temperature excursions in time ($\ln t$) of two thermometers at different radial distances, r_1 and r_2, from (1) a hot wire (W1, W2) and (2) a hot strip (S1, S2) heat source. The curves indicated as WL and SL are the Quasi-linear approximations, and WD and SD are the related QSS signals. The times denoted as $t_{\min}^{W2}$ and $t_{\min}^{S2}$ are the onset times of the QSS hot wire and the QSS hot strip techniques, respectively.

by homogeneous linear isothermal or adiabatic boundary conditions. This remarkable effect has already been discussed in detail in Ref. 1; if boundary conditions are isothermal (first kind) or convective (third kind), the QSS mode turns into the steady-state mode (see above), i.e., the output signal does not change with time. In these two cases, Eq. (12) of course breaks down while Eq. (5) still remains valid. If boundary conditions are adiabatic (second kind), the QSS mode turns into the "calorimetric" mode. Now, the temperature difference considered here is given by [1]

$$\Delta' T^{\mathrm{a}} = \frac{\Phi}{4\pi L\lambda}\left(\ln \varepsilon^2 + \frac{r_1^2(1-\varepsilon^2)}{R^2}\right) = \frac{\Phi}{4\pi L\lambda}(\ln \varepsilon^2 + \varphi). \tag{14}$$

The superscript "a" stands for adiabatic (boundary conditions). Compared with Eq. (5), there is an additional term, φ, on the right-hand side of Eq. (14).

$$\varphi = \frac{r_1^2 - r_2^2}{R^2} < 1. \tag{15}$$

As expected, for $r_1 = r_2$, both terms φ and $\ln \varepsilon$ vanish. For $R \gg \sqrt{|r_1^2 - r_2^2|}$, only φ dies out. This is the case for typical values of interest of r_1, r_2 and R (e.g., for $r_1 = 3.5\,\mathrm{mm}$, $r_2 = 10.5\,\mathrm{mm}$, and $R = 30\,\mathrm{mm}$ it follows $\varphi = -0.1$, cf. Fig. 1). Otherwise, φ has to be applied as a correction factor. In practice, the QSS mode still works under adiabatic boundaries. Then, Eq. (9) attains a form that is linear in t

$$\Delta t^{\mathrm{a}} = \frac{R^2}{4a}(\ln \varepsilon^2 + \varphi). \tag{16}$$

Substituting Eq. (15) into Eq. (13) yields

$$\Delta' T^{\mathrm{a}} = \frac{\Phi}{4\pi L\lambda}\frac{4a\Delta t^{\mathrm{a}}}{R^2} \tag{17}$$

from which with $\pi R^2 L = V$ and $a/\lambda = 1/(\rho c_{\mathrm{p}}) = V/(m c_{\mathrm{p}})$, directly emerges

$$c_{\mathrm{p}} = \frac{\Phi}{m}\left(\frac{\Delta' T}{\Delta t^{\mathrm{a}}}\right)^{-1}. \tag{18}$$

Here, m denotes the mass of the specimen whose specific heat, c_{p}, can be determined according to Eq. (18).

So far, the results show that a QSS run can be performed for the same task at each of the three different boundary conditions discussed.

Furthermore, once settled, the QSS output signal is constant so that there might be no time limit for an experiment. From practical aspects, now the question arises which of the three boundaries will produce the best data in an experiment.

A very important aspect here is to look at the dissimilar temperature excursions of the specimen at the different boundaries.

At isothermal or appropriate convective boundary conditions, the specimen temperature, $T_W(t)$, can easily be maintained constant. At adiabatic boundaries, however, after some time, $T_W(t)$ will increase linearly without bound because the specimen cannot release any heat to the surroundings. In contrast to one of the fundamental assumptions of the above briefly discussed ideal theory, in practice, the thermal conductivity of matter generally is not a constant but depends on temperature, $\lambda = \lambda(T)$. Hence, the thermal conductivity, $\lambda = \lambda(T(t))$, of the specimen will continuously change throughout an adiabatically bounded experiment. That is why in thermal transport properties measurements the temperature of the outer surface of the specimen is maintained constant during a run. In transient experiments, it is good practice to limit the temperature excursion of the specimen to about 2 K or even less. However, since the QSS signal appears as the pseudo-function $\lambda = \lambda(t)$, a run at adiabatic boundaries might provide the thermal conductivity as a function of temperature.

The above analysis can easily be extended to the THS technique. As has been shown in some detail in Ref. 1, both working equations, Eqs. (7) and (12), remain valid for this closely related method as long as $r_1, r_2 \geqslant D$. Here, D is the width of the strip. However, there is a remarkable difference between both transient techniques while used in the QSS mode. The onset of the QSS mode of a hot strip setup, the time $t_{\min}^{S2}$, is significantly smaller than that, $t_{\min}^{W2}$ (cf. Eq. (6)), for a hot wire arrangement [2]

$$t_{\min}^{S2} \geqslant \frac{r_2^2}{a}. \tag{19}$$

(cf. Fig. 1). According to Ref. 9, in the case of the THW technique, the signals at $r = r_1$ ("W1") and $r = r_2$ ("W2") are governed by

$$T^W(r,t) = T_0^i + \frac{\Phi_0}{4\pi L\lambda} \ln\left(\frac{R}{r}\right)^2 - 4\sum_{n=1}^{\infty} \frac{J_0(\mu_n r/R)}{\mu_n^2 J_1^2(\mu_n)} \left[\frac{\Phi_0}{4\pi L\lambda} + \frac{1}{2} T_0^i \mu_n J_1(\mu_n)\right] \exp\left(-\frac{\mu_n^2 at}{R^2}\right). \tag{20}$$

The eigenvalues are $J_0(\mu) = 0$ and $J_1(\mu) = 0$. In the case of the THS method ("S1" and "S2"), the above result can be modified to

$$T^{\mathrm{S}}(r,t) = T^{\mathrm{W}} + \frac{\Phi_0}{2\sqrt{\pi}L\lambda}\left\{\tau\,\mathrm{erf}(\tau^{-1}) - \frac{\tau^2}{2\sqrt{\pi}}\left[1-\exp(-\tau^{-2})\right]\right\} \tag{21}$$

as long as $R > rD$. In this equation, the additional term on the right-hand side represents the effect of the strip geometry on the temperature field of a line heat source, T^{W} (cf. Refs. 10 and 11). Here, $\tau = \sqrt{4at}/r$. Figure 1 shows both QSS signals, depicted as "WD" (Eq. (20)) for the THW technique and as "SD" (Eq. (21)) for the THS technique. While the onset of the linear portion of the THW signal of thermometer T2 occurs at $t_{\min}^{\mathrm{W2}} \leqslant 1985\,\mathrm{s}$ in the THS mode, the same thermometer will respond even at $t_{\min}^{\mathrm{S2}} \leqslant 221\,\mathrm{s}$.

In the case $t \to \infty$, which here is identical with the steady-state condition, Eq. (21) turns into the following simple form [11]:

$$\Delta T^{\mathrm{i}}(r, t\to\infty) \approx \frac{\Phi}{4\pi L\lambda}\left[\ln\left(\frac{R}{r}\right)^2 + 3\right]. \tag{22}$$

The superscript "i" stands for isothermal (boundary conditions).

Setting $r = r_1$ in Eq. (22) and combining this result with Eq. (5) yields an expression for the radial position of the second thermometer, r_2, in terms of the stationary temperature drop, $\Delta' T^{\mathrm{i}}$, between both thermometers, T1 and T2, on the one hand and the steady-state temperature, ΔT^{i} on the other hand

$$r_2 = r_1\,\exp\left\{\frac{\Delta' T^{\mathrm{i}}}{\Delta T^{\mathrm{i}}}\left[\ln\left(\frac{R}{r_1}\right) + \frac{3}{2}\right]\right\}. \tag{23}$$

From this result, criteria of an optimal design of a QSS sensor can be derived (see Section 3).

3. EXPERIMENTAL SETUP

A QSS experiment involves measuring the temperature at two stations inside a cylindrical specimen that conducts the heat generated by an embedded Joule heat source. This heater may either be a thin wire of radius r_0 or a metal strip of width D. For solids, a strip offers better performance than a wire because of the smaller density of heat flow, Φ/A, at its larger surface A and the smaller time lag prior to the onset of the QSS mode.

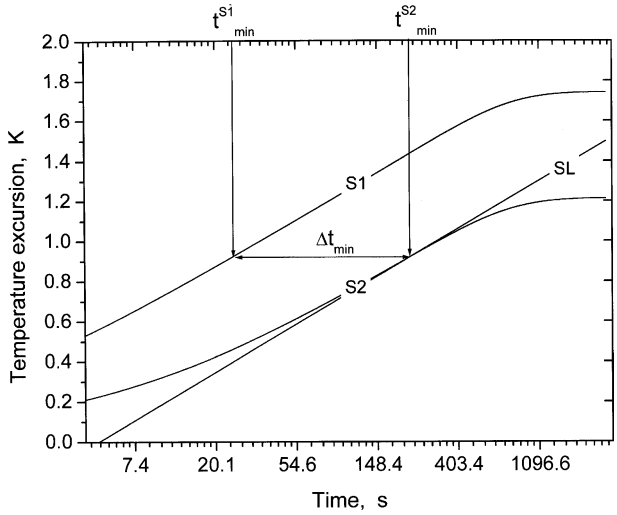

Fig. 2. Calculated temperature excursions in time ($\ln t$) of two thermometers at different radial distances, r_1 and r_2, from a hot strip heat source. The time shift between both signals (S1, S2) is indicated (same parameters as Fig. 1).

To establish the temperature measurement at two different stations of a THS arrangement, obviously, there are two simple ways. First, in a standard THS setup the strip serves as a resistance thermometer (cf., e.g., Refs. 2 and 10). By adding an extra temperature sensor, T2, at a known distance from the strip, this setup is readily expanded to a QSS arrangement (Fig. 2). Optionally, two individual temperature sensors, T1 and T2, can be employed on one or both sides of the strip (Fig. 3). In practice, the latter variation of two thermometers is more advantageous; it allows

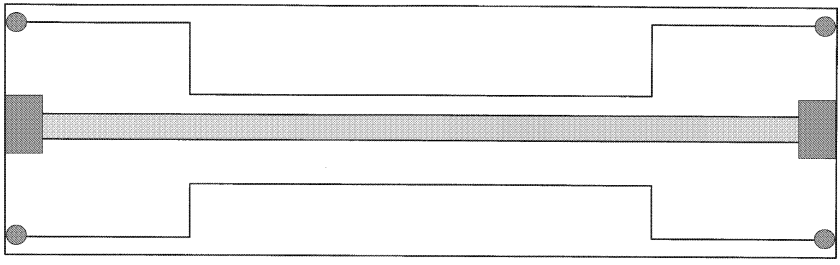

Fig. 3. Sketch of the QSS λ-sensor. The strip (center) is made from manganin®, both temperature sensors (cold wires) are made from platinum (not to scale).

elimination of two different sources of (model) error arising from major discrepancies between a real THS setup and its underlying ideal mathematical model: (1) From theory, a homogeneous temperature profile along the longitudinal axis of the strip is assumed. In an experiment, however, this profile is more or less curved at both ends of the strip because of heat losses to the surroundings including the electrical leads (end effect). By placing both thermometers next to the central part of the strip (see Fig. 3) this source of error can easily be removed. (2) In order to simplify a THS experiment, generally, a constant current I_0 is fed to the strip rather than a constant power, $P = R_S I^2$, as presumed by theory. By this means, however, the power consumption may significantly rise throughout the run due to a temperature dependent increase in the resistance, $R_S = R_S(T)$, of the strip. By using two thermometers, the strip can be operated in its heater function only. Thus, an alloy of vanishing temperature coefficient of electrical resistance like, e.g., manganin® ($\alpha = 0.00001\,\mathrm{K}^{-1}$), applies well as a source material for the strip.

The following analysis of the major sources of error of the QSS technique is based on an experimental arrangement of a strip and two separate temperature sensors. Boundary conditions are maintained isothermal to keep the working temperature, $T_W = T_0$, constant. For this setup, both QSS working equations, Eqs. (7) and (12), apply. Hence, there are two slightly different ways to perform a thermal conductivity measurement. According to Eq. (7), the temperature difference $\Delta' T(t)$ has to be recorded for a known ratio of r_1 and r_2 while otherwise, i.e., Eq. (12), the time shift $\Delta \ln t$ has simultaneously to be determined from both individual temperature excursions (cf. Fig. 2). Here, the first procedure, Eq. (7) is taken as the basis of a measurement.

The λ-sensor used for the experiments is depicted schematically in Fig. 3. Sandwiched between two polyimide (Kapton®) foils (each with a thickness $\nu = 25\,\mu\mathrm{m}$) there are a strip made from manganin® ($\nu = 10\,\mu\mathrm{m}$) and two thin platinum wires ($\varnothing = 10\,\mu\mathrm{m}$) as the resistance thermometers. The electrical resistivity of the central part of these temperature sensors is $R_T = 18\,\Omega$ each. For any given set of dimensional parameters r_1, r_2, D, and R of the sensor and the specimen, respectively, the following must be valid $D \leqslant r_1 < r_2 \leqslant R$ (see Tables I and II).

The specimen used here to confirm the results of the uncertainty assessment is a parallelepiped consisting of two identical halves. The material is polymethyl methacrylate (PMMA, Plexiglas®, Type GS, Degussa Röhm Plexiglas GmbH, Germany). This type of PMMA is a candidate reference material of PTB. The specimen has been cut from the reference material stock. To minimize thermal contact resistances, those surfaces contacting the λ-sensor were polished carefully. The sample is

Table I. Geometrical Dimensions of the λ-Sensor (see text)

Strip	Symbol	Dimension (mm)
Length	L	100.0
Width	D	3.0
Thickness	ν	0.01
Distance to T1	r_1	3.5
Distance to T2	r_2	10.5

Table II. Geometrical Dimensions of the Specimen (One Half) (see text)

Specimen	Symbol	Dimension (mm)
Length	L	100.0
Width	R	30.0
Thickness	V	15.0

contained inside a metallic sample holder that itself is immersed in a thermostated bath.

For any given set of dimensional parameters, r_1, r_2, and L of the sensor, the input power, $P = UI_0 = \Phi$, to the strip should be adjusted to the specimen's expected thermal conductivity in order to generate a proper output signal (see Section 4). As has been mentioned above, the temperature excursion $T_1(r_1, t)(> T_2(r_2, t))$ should not exceed 2 K.

4. MODEL AND MEASUREMENT ERRORS

According to the working equation, Eq. (7), the thermal conductivity is measured as a pseudo-function in time. In practice, a series of equivalent values, $\lambda(t_i) = \lambda_i$, of the measurand are recorded at a constant clock rate of the digital voltmeter. Thus, each individual result is subject to systematic, type-B, and random, type-A, uncertainties. Systematic uncertainties have the same effect on the measurement each time a sample, λ_i is acquired. Random uncertainties vary from sample to sample. In accordance to the ISO Guide, once estimated, both uncertainties are handled in the same manner; they are root-sum squared.

To calculate the systematic uncertainties first, seven parameters, U, I_0, T_1, T_2, L, r_1, and r_2 have to be taken into account. The first four parameters stem from the electrical part of the setup, including both temperatures that are determined by resistance thermometry. The following three-dimensional parameters depend on the type of the sensor used and, thus, are fixed by their layout. Generally, they are subject to thermal expansion, in case of L and D, of the metal of the strip (manganin) and,

in case of the base material, of the polyimide foil. In the following, however, room temperature is assumed. It is further assumed that the polyimide foil is thin enough not to have a significant effect on the result of the measurement. Moreover, as a reference, polymethyl methacrylate is used here because of its thermal conductivity that differs only slightly from that of the foil ($\lambda_{\text{Kapton}} = 0.2\,\text{W}\cdot\text{m}^{-1}\cdot\text{K}^{-1}$). The thermal contact resistance between the foil and the specimen is neglected. The influence of the insulating base material of the sensor on the result of a measurement and on the overall uncertainty is difficult to derive analytically. Therefore, numerical studies using finite element methods are under way. Results obtained so far show that, in the present case, the uncertainty due to the non-vanishing thickness of the foil can be assessed to be less than 0.1%.

Finally, the working equation itself can give rise to errors because of ideal assumptions and approximations made to derive it from the underlying fundamental partial differential equation.

4.1. Linear Model Error

A QSS setup can be analytically treated only for the above made assumption that the exponential integral, $-\text{Ei}(-z)$, on the right hand side of the THW ideal model equation, Eq. (1), may be represented sufficiently precise by the first two terms of the related McLaurin series. This, however, is true only for $r^2/at \ll 1$. Due to the asymptotic form of the (quasi) linearization of Eq. (2), there is a certain deviation from the ideal model, known as the linear model error (Refs. 2 and 3). In THW and THS experiments this error may significantly increase the uncertainty of the measurands λ and a.

To analyze the implications of the model error for the uncertainty of a QSS run, the working equation, Eq. (5), is recalculated. Now, two more terms of the series are retained as represented by Eq. (2). The asymptotic relation governing QSS signals is expressed as

$$\Delta' T(r,t) = \frac{\Phi}{4\pi L\lambda}\left[\ln\left(\frac{r_2^2}{r_1^2}\right) - \frac{\left(r_2^2 - r_1^2\right)}{4at} + \frac{1}{4}\left(\frac{\left(r_2^2 - r_1^2\right)}{4at}\right)^2 \mp \ldots\right]. \quad (24)$$

Obviously, all terms of the remainder die out for $(r_2^2 - r_1^2)/(4at) \ll 1$. For $r_2 > \sqrt{2}r_1$ the difference of the squares, $\left(r_2^2 - r_1^2\right)$, is larger than r_1^2 itself. Hence, in this case it takes more time for the QSS signal to settle. This result fully agrees with the approximation in Eq. (6), i.e., the output signal $\Delta' T = T_1 - T_2$ will not be sufficiently constant before the second input signal, ΔT_2, starts to vary as $\ln t$. Once settled, the QSS signal is prac-

tically free of any linear model error. Hence, the model error is self-validating; for the case where at least one single temperature signal, $T_1(t)$ or $T_2(t)$, cannot be described by the simple quasi-linear equation, Eq. (4), the composed QSS signal will not be sufficiently constant in time.

4.2. Power

The heat flow, Φ, generated by the strip is determined from its electric input power, $\Phi = P = U(R_S)I_0$. The voltage drop, U, across the strip is directly measured and the current, I_0, is determined indirectly from the voltage drop, U_R, across a calibrated four-pole standard resistor $R_R = 1\,\Omega$. As has been mentioned above, despite a constant current operation there is no significant change in the power consumption of the strip because of the very small temperature coefficient of its electrical resistance.
The following working relation holds

$$P = UU_{\mathrm{R}}/R_{\mathrm{R}}. \tag{25}$$

The variance of the quantity P is given by

$$u^2(P) = \left(\frac{U_{\mathrm{R}}}{R_{\mathrm{R}}}\right)^2 u^2(U) + \left(\frac{U}{R_{\mathrm{R}}}\right)^2 u^2(U_{\mathrm{R}}) + \left(\frac{UU_{\mathrm{R}}}{R_{\mathrm{R}}^2}\right)^2 u^2(R_{\mathrm{R}}). \tag{26}$$

Here, the variance of the standard resistor, $u^2(R)$, is obtained from the calibration certificate. The variances of the voltmeter, $u^2(U)$ and $u^2(U_{\mathrm{R}})$, are taken from the manufacturer specifications that have been verified by in-house calibration. All three variances have been calculated according to type-B method

$$u^2(P) = 2.3 \times 10^{-8}\,\mathrm{W}^2.$$

4.3. Temperature

The maximum temperature range of the sensor is predetermined by the base material which can be, e.g., a polymer, a ceramic, or a mica foil. Here, the high performance polyimide Kapton® is taken that can be used at temperatures from –270 up to 250°C.

At present, the accessible temperature range for a QSS run at PTB is from −80 to 220°C. During a run at the controlled working temperature, T_0, the temperature excursion of the specimen is limited to $T = T_0 + 2\,\mathrm{K}$.

The temperatures T_1 and T_2 are individually measured by the two platinum wires of the sensor (see Fig. 3). These thermometers were calibrated against a reference standard Pt-25 resistor. The observed mean values of 15 measurements of each of four different temperatures, measured as voltage drop and converted into temperatures in accordance with the individual calibration tables show a maximum variance of

$$u^2(T) = 82 \times 10^{-6}\,\mathrm{K}^2.$$

4.4. Ambient Temperature Variation

The experiments are carried out inside a well-stirred thermostated bath. Its randomly distributed temperature variations are determined to be $\pm 10 \ldots 15\,\mathrm{mK}$. Any change in the working temperature, T_W, causes a departure in the measured voltage signals of T1 and T2

$$\delta U_i^{\mathrm{T}} = \alpha U_0 \frac{dT_{\mathrm{W}}}{dt} t_{\mathrm{i}}. \tag{27}$$

Depending on the period of the temperature–time variations of the bath and the mutual distance between the two thermometers, the fluctuations in the temperature difference $\delta\left(\Delta' T\right) = \delta U_{\mathrm{i}}^{\mathrm{T1}} - \delta U_{\mathrm{i}}^{\mathrm{T2}}$ generally reveal a complex behavior. They may even vanish. This error is treated as part of the random uncertainty of the λ_i-readings (see Section 4.5).

4.5. Dimensional Parameters

The three dimensional parameters to be taken into account are L, length of the hot strip, and the individual distances, r_1 and r_2, of both thermometers from the longitudinal axis of the strip. All three lengths were determined at room temperature using a measuring microscope. The half width of bounds is 1/100 mm for a rectangular probability distribution.

5. STANDARD UNCERTAINTY

The physical process of a QSS measurement is governed by the expression,

$$\lambda(T_W) = \frac{U I_0}{2\pi L \left[T(r_1, t) - T(r_2, t)\right]} \left(\ln r_2 - \ln r_1\right). \tag{28}$$

It is assumed that both temperature excursions, $T_1(t) = T(r_1, t)$ and $T_2(t) = T(r_2, t)$, and both (constant) radii, r_1 and r_2, are measured separately. Furthermore, r_i and not $\ln r_i$ is determined experimentally. Then, according to the GUM [5], the standard uncertainty of the measurand is composed from the relative uncertainties, $u(x_\mathrm{i})/x_\mathrm{i}$, in the measured variables x_i as follows:

$$\left(\frac{u(\lambda)}{\lambda}\right)^2 = \left(\frac{u(U)}{U}\right)^2 + \left(\frac{u(I_0)}{I_0}\right)^2 + \left(\frac{u(L)}{L}\right)^2 + \left(\frac{u(T_1)}{T_1 - T_2}\right)^2 + \left(\frac{u(T_2)}{T_1 - T_2}\right)^2 + \left(\frac{u(r_1)}{r_1 \ln \varepsilon}\right)^2 + \left(\frac{u(r_2)}{r_2 \ln \varepsilon}\right)^2 + \left(\frac{\delta_\mathrm{M}\lambda}{\lambda}\right)^2 + \left(\frac{\delta_\mathrm{R}\lambda}{\lambda}\right)^2. \tag{29}$$

As a result of the additive form of the expression, Eq. (28), the relative uncertainty in λ depends not only on the component uncertainties in the variables U, I_0, T_1, T_2, L, r_1, and r_2 but also on the values of both temperatures and radii. For these two pairs of parameters the so-called uncertainty magnification factors, UMF_i are different from 1

$$\left(\frac{u(\lambda)}{\lambda}\right)^2 = \left(\frac{u(U)}{U}\right)^2 + \left(\frac{u(I_0)}{I_0}\right)^2 + \left(\frac{u(L)}{L}\right)^2 + \left(\frac{T_1}{T_1 - T_2}\right)^2 \left(\frac{u(T_1)}{T_1}\right)^2 + \left(\frac{T_2}{T_1 - T_2}\right)^2 \left(\frac{u(T_2)}{T_2}\right)^2 + \left(\frac{1}{\ln \varepsilon}\right)^2 \left(\frac{u(r_1)}{r_1}\right)^2 + \left(\frac{1}{\ln \varepsilon}\right)^2 \left(\frac{u(r_2)}{r_2}\right)^2 + \left(\frac{\delta_\mathrm{M}\lambda}{\lambda}\right)^2 + \left(\frac{\delta_\mathrm{R}\lambda}{\lambda}\right)^2. \tag{30}$$

According to Ref. 14, the uncertainty magnification factors that multiply the relative uncertainties of the variables are defined as

$$\mathrm{UMF}_\mathrm{i} = \frac{X_\mathrm{i}}{\lambda}\frac{\partial \lambda}{\partial X_\mathrm{i}}, \quad \lambda = \lambda\left(X_1, X_2, X_3, \ldots, X_\mathrm{j}\right). \tag{31}$$

For further discussions on the UMF_i, see Section 5.1.

In Eq. (30) both uncertainties in temperature are equal, $u(T_1) = u(T_2) = u(T)$. The term next to the last one on the right-hand side, $\delta_\mathrm{M}\lambda/\lambda$, represents the uncertainty due to the linear model error. As has been shown already, it may further be neglected. The last term on the right-hand side, $\delta_\mathrm{R}\lambda/\lambda$, denotes the uncertainty caused by nonsystematic effects on each individual reading λ_i.

Typically, the measurand is obtained as a series of N individual observations, $\lambda_\mathrm{i}(T_\mathrm{W})$, taken over a period in time at equally spaced points t_i.

$$\lambda_\mathrm{i}(T_\mathrm{W}) = \frac{U I_0}{2\pi L\left[T(r_1, t_\mathrm{i}) - T(r_2, t_\mathrm{i})\right]}\left(\ln r_2 - \ln r_1\right), \quad \mathrm{i} = 1, \ldots, N. \tag{32}$$

Although a QSS instrument is operating at a "steady" value of λ, the single readings are not exactly constant due to random uncertainties, $\delta_R\lambda/\lambda$. The final result, the optimum value of the thermal conductivity, is derived from the arithmetic mean,

$$\lambda_{opt}(T_W) = \frac{1}{N}\sum_{i=1}^{N}\lambda_i(T_W). \tag{33}$$

The dispersion of the random distribution of the measurand, $\lambda_i(T_W)$, is given by the related standard deviation from which the uncertainty is derived.

5.1. Uncertainty Magnification Factor

The uncertainty magnification factor for a given parameter indicates the influence of the uncertainty in that variable on the uncertainty in the result [12]. In Eq. (30), the UMF of temperature, e.g., T_1, is given by

$$UMF_{T1} = \frac{T_1}{T_1 - T_2} = \frac{T_1}{\Delta' T}, \tag{34}$$

while the UMF for both radii is

$$UMF_r = \frac{1}{\ln \varepsilon} = \frac{1}{\ln(r_2/r_1)}. \tag{35}$$

Obviously, the above factors should be as small as possible to assure a minimum in the overall uncertainty in λ (see Fig. 4). For a given value of 0.1% for each relative uncertainty in T and r_2, both UMF's were calculated over a range of ε from 1 to 11. Figures 5 and 6 show the results along with the QSS offset time t_{min}^{S2} (depicted in Fig. 5 as t_{min}) and the QSS signal (depicted in Fig. 6 as ΔT). The uncertainty percentage contribution of both parameters discussed varies from 100 to 0.3% within the relatively small range covered. Throughout this range, the QSS signal grows with increasing distance of thermometer T2 from the other thermometer because of a declining signal of T2, $T_2(t) \to T_0 = \text{const.}$ (Fig. 6). However, to the same extent, the onset, t_{min}^{S2} of the quasi-steady mode is shifted to longer times (Fig. 5). In the limit $r_2 = R$ and $T_2(t) = T_0$ (which is not shown in the diagram) the QSS mode turns either into the steady-state mode (see above) if boundary conditions are isothermal or adequately convective or into a "calorimetric" mode if adiabatic boundaries are present.

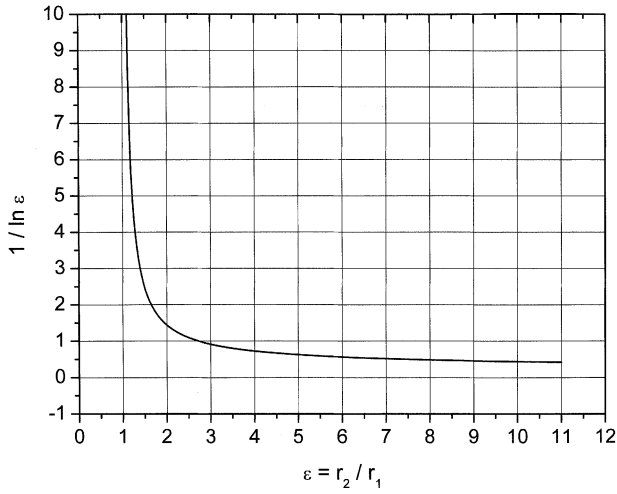

Fig. 4. Uncertainty magnification factor UMF_r of the parameter "radius" versus ratio of radial distances, ε, of the thermometers.

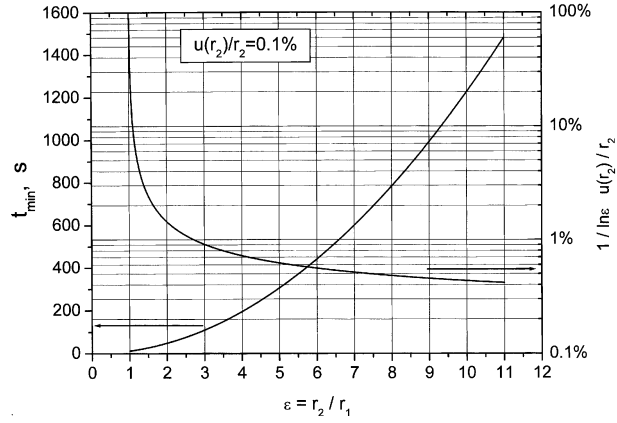

Fig. 5. QSS onset time t^{S}_{min} (left y-axis) and percentage uncertainty of radius r_2 (right y-axis) versus ε (see text).

5.2. Sensor and Experiment Design

From the above briefly discussed UMF's, some criteria for the design of an optimal QSS sensor and of the best suited experiment, concerning temperatures and the onset of the QSS mode, can be derived. The UMF for r_i is a function of r_i itself and grows without bound as r_2/r_1 approaches unity (Fig. 4). Conversely, as $r_2/r_1 \to \infty$, UMF_r vanishes. This

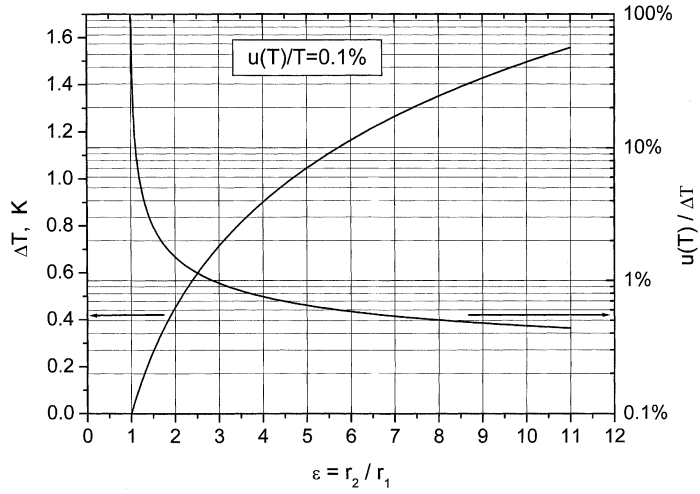

Fig. 6. Temperature drop between the two thermometers at r_1 and r_2, respectively (left y-axis) and percentage uncertainty of temperature (right y-axis) versus ε (see text).

behavior still is quite clear because, in the first case, the QSS mode breaks down ($r_2 = r_1$) and, in the second case, this mode does not start at all ($t \to \infty$). Whereas, the situation becomes more complicated when taking into account that each of both UMF's of temperature, $\mathrm{UMF_{T1}}$ and $\mathrm{UMF_{T2}}$, depend on the UMF of radius, UMF_r. From Eqs. (5) and (34),

$$\mathrm{UMF_{T1}} = \frac{T_1}{k \ln \varepsilon} = \frac{T_1}{k}\mathrm{UMF_r}, \quad \Delta' T = k \ln \varepsilon, \quad k = \frac{\Phi}{2\pi L \lambda} = \text{const.}, \tag{36}$$

directly emerges. For a fixed value of r_1, the temperature difference increases with growing r_2. However, as r_2 becomes larger, the onset of the QSS mode is shifted in time since by Eq. (19)

$$t_{\min}^{\mathrm{S2}} \propto r_2^2 \tag{37}$$

is valid. Here again, for $r_2 = r_1$ (cf. Eq. (11)) the QSS mode breaks down. Obviously, there are various compromises available that individually apply for different experimental situations. By varying the position, r_2, of the thermometer T2, the overall uncertainty, $u(\lambda)$, the onset of the QSS mode, $t_{\min}^{\mathrm{S2}}$, and/or the temperature difference, $\Delta' T$, can be controlled.

The strategy for the brief parametric study on an optimum sensor design followed is to simultaneously look at the two different pairs of variables (1) $\Delta' T$ and UMF_T (Fig. 6) and (2) $t_{\min}^{\mathrm{S2}}$ and UMF_r (Fig. 5) in order

to minimize the overall uncertainty in the measurand. Alternative objectives could be, e.g., to minimize the onset time or the temperature drop between the thermometers for an uncertainty that consequently is higher.

First of all, there are three fundamental criteria for the layout of the sensor that have to be fulfilled. The parameters L, D, R, and r_1 are fixed in a way that

(1) $L \gg D$,
(2) $D \leqslant r_1 < r_2 < R$,
(3) $T_2(t) < T_1(t) < 2\,\mathrm{K}$.

Assumption (1) ensures that there is a family of concentric *near-circular* isotherms around the strip source. According to (2), both thermometers are located inside this family of isotherms (cf. Refs. 1 and 2). Finally, (3) is good practice for transient measurements of thermal conductivity because $\lambda = \lambda(T)$.

All values that have been assigned to the fixed parameters are listed in Tables I and II. Only the radius r_2 remains to be determined; to achieve a relative uncertainty in temperature and radius of less than, let's say, 1% each, the ratio ε has to be equal to at least 3 (Figs. 5 and 6). For $\varepsilon_0 = 3$, i.e., $r_2 = 10.5\,\mathrm{mm}$, the QSS onset will be at $t_{\min}^{S2} \approx 100$ s (Fig. 5) and the temperature drop between the two thermometers will be $\Delta' T^{\mathrm{i}} \approx 0.72\,\mathrm{K}$ (Fig. 6). This last result together with $T_1(t \to \infty) = \Delta T^{\mathrm{i}} \approx 2\,\mathrm{K}$ (see condition (3)), inserted into Eq. (23), yields

$$r_2 = r_1 \exp\left\{\frac{\Delta' T^{\mathrm{i}}}{\Delta T^{\mathrm{i}}}\left[\ln\left(\frac{R}{r_1}\right) + \frac{3}{2}\right]\right\} = 10.1\,\mathrm{mm},$$

which agrees well with the above chosen ratio ε_0. For values of r_2 ranging from 3.6 to 15 mm, the resulting temperature difference $\Delta' T^{\mathrm{i}}$ is plotted in Fig. 7. The parameters used to calculate $\Delta' T^{\mathrm{i}}$ are the same as for the uncertainty budget given in Section 5.3.

Finally, the electrical parameters of the experiment can be assessed; Eq. (5) is rearranged for the input power of the strip,

$$\Phi = R_{\mathrm{S}} I_0^2 = 2\pi L \lambda \Delta' T \left[\ln\left(\frac{r_2}{r_1}\right)\right]^{-1}. \tag{38}$$

The already known dimensional parameters are inserted along with an estimate of the thermal conductivity of the specimen, here, PMMA. For a polymer at room temperature, the thermal conductivity should be $\lambda \approx 0.2\,\mathrm{W \cdot m^{-1} \cdot K^{-1}}$. Then, for the power input of the strip, the value $\Phi \approx$

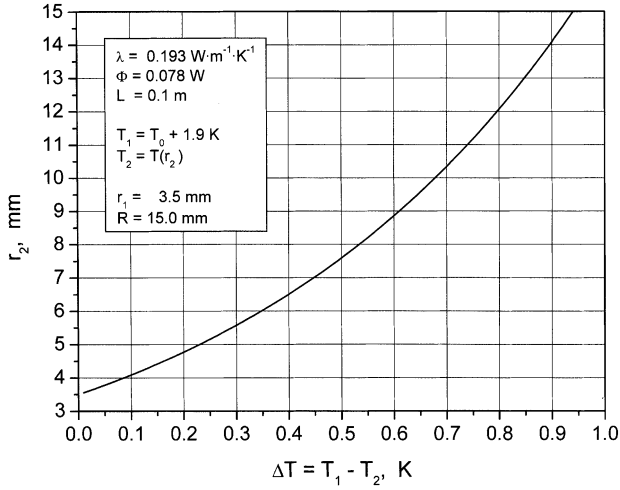

Fig. 7. Calculated radial distance from strip of thermometer T2 versus temperature difference between both thermometers T1 and T2.

0.080 W is estimated. Thus, a current of $I_0 \approx 170$ mA has to be fed to the strip of resistance $R_S = 2.9\,\Omega$.

5.3. Uncertainty Budget

All results of the component uncertainties, $u(x_i)$, are listed in Table III together with the experimental parameters of a measurement on PMMA at room temperature. Obviously, the actual experimental parameters agree very well with those estimated above. Table III additionally lists the numerical values of the sensitivity coefficients, $m_i = \partial\lambda/\partial x_i$, and a percentage index that describes the contribution of each component to the overall uncertainty.

The result of the measurement is $\lambda = 0.1928 \pm 7.2 \times 10^{-3}\,\mathrm{W{\cdot}m^{-1}{\cdot}K^{-1}}$. The uncertainty (3.7%) is based on a standard uncertainty mutliplied by a coverage factor of $k = 2$ which provides a level of confidence of approximately 95% (20 to 1 odds).

The result mentioned agrees very well with the preliminary reference value of this material that is given as $\lambda = 0.1934 \pm 12 \times 10^{-3}\ \mathrm{W{\cdot}m^{-1}{\cdot}K^{-1}}$. Further measurements at temperatures other than room temperature are under way. The last column of Table III, labeled as 'Index', lists the fractions of all component uncertainties except for the random uncertainty $\delta_R\lambda$. N denotes the total number of readings, λ_i $(i = 1, \ldots, N)$.

Table III. Uncertainty Budget

Symbol x_I	Quantity	Value	$u(x_i)$	Type	Degree of Freedom	Sensitivity Coefficient	$\mu(x_i)$ ($W \cdot m^{-1} \cdot K^{-1}$)	Index (ms%)
P	Rate of heat flow	0.0784 W	150×10^{-6} W	A	15	2.5	370×10^{-6}	1.1
L	Length of strip	0.1 m	5.77×10^{-6} m	B/rect.	∞	-1.9	-11×10^{-6}	0.0
T_1	Temperature	1.91°C	9×10^{-13} K	A	15	-0.27	-2.4×10^{-3}	49.1
T_2	Temperature	1.20°C	9×10^{-13} K	A	15	0.27	2.4×10^{-3}	49.1
r_1	Radial distance	3.5 mm	5.77×10^{-6} m	B/rect.	∞	17.0	96×10^{-6}	0.1
r_2	Radial distance	10.5 mm	5.77×10^{-6} m	B/rect.	∞	-50.0	-290×10^{-6}	0.7
$\delta_R \lambda$	Random unc.		1×10^{-3}	A	N	1	1×10^{-3}	nn
λ	Thermal conductivity	0.192_8 $W \cdot m^{-1} \cdot K^{-1}$	3.57×10^{-3} $W \cdot m^{-1} \cdot K^{-1}$	comb. $k=1$	31			

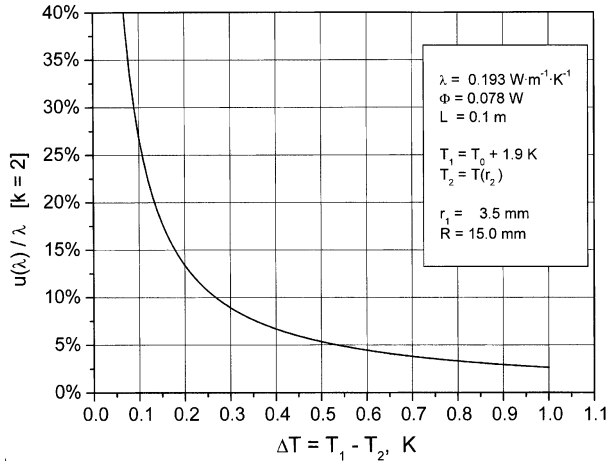

Fig. 8. Standard uncertainty in thermal conductivity for given λ-sensor parameters versus temperature drop between the two thermometers at r_1 and r_2, respectively.

From Table III it is immediately apparent that the effect of the uncertainty of the electrical and dimensional parameters is negligible relative to the influence of $u(T)$. The results listed under 'Index' reveal that both temperature uncertainties are by far the largest components of the overall uncertainty despite their small sensitivity coefficient. This behavior is not surprising; it was already found for the THS, THW, and the guarded hot plate techniques (Refs. 2–4).

For the above experiment on PMMA, the percentage standard uncertainty ($k = 2$) of thermal conductivity has been assessed in terms of the temperature difference between both thermometers ranging from 0.05 to 1 K. The results in Fig. 8 show the considerable influence of this parameter on the uncertainty. To ensure an acceptable uncertainty in thermal conductivity of, let's say, $u(\lambda)/\lambda \leqslant 5\%$, the temperature difference has to be greater than 0.55 K. From Fig. 7 follows a minimal value of $r_2 \geqslant 8$ mm.

Despite their relatively great sensitivity coefficients, both radial distances r_1 and r_2 have only a minor contribution to the overall uncertainty. This effect might be underestimated here because thermal expansion has not been taken into account.

Comparing the above assessed uncertainty of the QSS technique with equivalent other methods like the guarded hot plate, GHP (1.9% from Ref. 4), the transient hot wire (5.8% from Ref. 3), and the transient hot strip (5% from Ref. 2) techniques reveals that the most precise instrument for

poor conducting solids still is the GHP apparatus. However, if a short measurement time at a reasonable uncertainty level is demanded the QSS method is able to compete with the transient techniques mentioned.

6. CONCLUSION

The present study analyzes the most significant sources of error of the newly developed QSS technique. The results are combined to the standard uncertainty of thermal conductivity, $u(\lambda)/\lambda = 3.7\%$, according to the ISO Guide. This value compares well with those found for the guarded hot plate (1.9%) THW (5.8%) and THS (5%) techniques. As has been found for the three other techniques mentioned here, again the temperature uncertainty contributes predominantly to the overall uncertainty in thermal conductivity.

Simultaneously, the assessment was used as an aid in designing a QSS sensor of minimal uncertainty and in planning the experiment. Such a sensor is used to verify the above mentioned standard uncertainty from a run on the candidate reference material polymethyl methacrylate.

It can be concluded that the new QSS technique will meet the requirements of good measurement uncertainty if the QSS signal is greater than 0.7 K.

REFERENCES

1. U. Hammerschmidt, *Int. J. Thermophys*. (*in press*).
2. U. Hammerschmidt and W. Sabuga, *Int. J. Thermophys.* **21**:217 (2000).
3. U. Hammerschmidt and W. Sabuga, *Int. J. Thermophys.* **21**:1255 (2000).
4. U. Hammerschmidt, *Int. J. Thermophys.* **23**:1551 (2002).
5. ISO, *Guide to the Expression of Uncertainty in Measurement* (ISO, Geneva, 1992).
6. K. D. Maglic, A. Cezairlyan, and V. E. Peletsky, eds., in *Compendium of Thermophysical Properties Measurement Methods*, Vol. 1: *Survey of Measurement Techniques* (Plenum Press, New York and London, 1984).
7. J. J. Healy, J. J. de Groot, and J. Kestin, *Physica* **82C**:392 (1976).
8. W. A. Wakeham, A. Nagashima, and J. V. Sengers, *Measurement of the Transport Properties of Fluids*, Vol. III (Blackwell Scientific, Oxford, 1992).
9. H. Tautz, *Wärmeleitung und Temperaturausgleich* (Verlag Chemie GmbH,Weinheim, 1971).
10. S. E. Gustafsson, E. Karawacki, and M. N. Khan, *J. Phys. D* **12**:1411 (1979).
11. U. Hammerschmidt, in *Proc* 24th *Int. Thermal Cond. Conf., Pittsburgh, 1997*, P.S. Gaal ed. (Technomic, Lancaster, Pennsylvania, 1999).
12. H. W. Coleman and W. G. Steele, in *Experimentation and Uncertainty Analysis for Engineers*, 2^{nd} Ed. (John Wiley, New York, 1998)